Anonymous Referee #2

This paper addresses the by now seemingly well established underestimation of coarse and giant dust particles by large-scale models. This is an important topic, as these particles are much more abundant than previously thought, such that models could be missing important effects on radiation, clouds, and biogeochemistry. The present paper tries to address this issue by using in situ measurements of dust size distribution over the North African source regions to parameterize the sizes of emitted dust in the WRF-Chem model and then comparing the results against. They find that the deposition velocity of
particles must be greatly reduced in order for the model to match measurements further from source regions, which further confirms previous findings in the literature that coarse dust deposits too quickly in models.

Overall, this is a useful contribution to the literature. I did find a series of issues with the description of the methods and results. None of them are serious enough to preclude publication and I'm hopeful that a next version would be suitable for publication. Nonetheless, major revisions are required.

We appreciate the positive feedback of the reviewer and we would like to thank him/her for the effort and expertise that he/she contributed towards reviewing our manuscript. We are grateful for the insightful comments and we tried to incorporate changes to reflect the provided suggestions.

Specific comments:

- **I think the paper should be clearer about the actual objective of the paper is or the scientific question it addresses. If this is just to "extend the parameterization the mineral dust cycle in the GOCART-AFWA dust scheme of WRF4.2.1 to include also coarse and giant particles" then this is pretty narrow and perhaps better suited for GMD or a similar journal. But it seems that the authors also investigate the reasons for why coarse and giant dust is underestimated by models, finding that particles settle much too fast in the model. I would suggest making this objective of the paper clearer, especially in the abstract and the end of the introduction.**

We agree with the reviewer's comment. Therefore, we modified the abstract and the introduction section, emphasizing more that the additional purpose of that work-apart from the development of a model that includes the fine,coarse and giant dust particles- is also to investigate the reasons behind the model overestimation of the dust particles' settling. The abstract section is given in lines 13, page 1 of the revised document:

"Dust particles larger than 20 μm in diameter have been regularly observed to remain airborne during long-range transport. In this work, we modify the parameterization of the mineral dust cycle in the GOCART-AFWA dust scheme of WRFV4.2.1, to include also such coarse and giant particles, and we further discuss the underlying misrepresented physical mechanisms which hamper the model in reproducing adequately the transport of the coarse and giant mineral particles. The initial particle size distribution is constrained by observations over desert dust sources. Furthermore, the Stokes' drag coefficient has been updated to account realistic dust particles sizes ($Re < 10^5$). The new code was applied to simulate dust transport over Cape Verde in August 2015 (AER-D campaign). Model results are evaluated against airborne dust measurements and the CALIPSO-LIVAS pure dust product. The results show that the modelled lifetimes of the coarser particles are shorter than those observed. Several sensitivity runs are performed by reducing artificially the particles' settling velocities in order to compensate underrepresented mechanisms, such as the non-spherical aerodynamics, in the relevant parameterization schemes. Our simulations reveal that particles with diameters of 5.5-17 μm and 40-100 μm are better represented under the assumption of a 80% reduction in the settling velocity (UR80) while particles with sizes ranging between 17μm and 40 μm are better represented in a 60% reduction

in settling velocity (UR60) scenario. The overall statistical analysis indicates that the best agreement with airborne in-situ measurements downwind (Cape Verde) is achieved with 40% reduction in settling velocity (UR40). Moreover, the UR80 experiment improves the representation of the vertical structure of the dust layers as those are captured by the CALIPSO-LIVAS vertically-resolved pure dust observations. The current study highlights the necessity of upgrading the existing model parameterization schemes of the dust life-cycle components towards improving the assessment of the dust-related impacts within the Earth-Atmosphere system."

Based on the reviewer's suggestion, we also modified the part of the introduction that summarizes the overarching goal of our study, the tools which have been utilized, and the justification and validity of our approach. The related part of the introduction is cited in line 95, page 4 of the revised document:

"In this work, we demonstrate for the first time a method for incorporating coarse and giant desert dust particles (D > 20 μm, following the definition of the dust modes proposed in Ryder et. al, (2019), into the Advanced Research Weather version of the Weather Research and Forecasting (WRF-ARW) model in conjunction with the GOCART (Ginoux, 2003) aerosol model and the Air Force Weather Agency (AFWA) dust emission scheme (LeGrand et al., 2019) (WRF-GOCART-AFWA model). After pinpointing that the model quickly deposits coarse and giant dust particles, we investigate the reasons behind those findings: We use sophisticated in situ PSD measurements to initialize the model over the sources and to evaluate the simulated PSD over the receptor areas. We also use pure-dust spaceborne retrievals to assess the model performance in terms of reproducing the vertical structure of the dust layers. In addition, we perform a series of sensitivity tests by reducing the settling velocity of mineral particles in the model and we investigate the concomitant effects on dust fields. "

- **I'm puzzled by the lengthy discussion of the inclusion of a new drag coefficient in section 2.1.2. I understand that a drag coefficient parameterization that is valid for larger Re number must be implemented since you're treating coarse and giant dust (with Re up to 10 or so), but I think the drag law you use (Eq. 14) is fairly standard. So rather than taking up the reader's finite attention with this lengthy description, I recommend you just state you implemented the drag coefficient law from Clift et al. (2005). Additionally, you should show that implementing this new**

drag coefficient law is actually important by including a plot of the new and old drag coefficients versus particle size.

One of the major and critical advancements in our work is the extension of the drag coefficient applicability for larger particles. This modification affects the simulated settling velocities and the particles' deposition rate. Despite the fact that the drag coefficient by Clift and Gauvin, 1971 is a standard drag coefficient, we have modified the way that the slip correction is applied compared to the WRF default version. In the WRF default code, the slip correction is applied unconditionally for any Re. However, in Mallios et al. (2020) it has been shown that the slip correction should be applied only in the Stokes regime Re<0.1. Thanks to this consideration (i.e., slip correction), a more realistic representation (i.e., large Re) of the settling velocities of larger particle sizes is achieved. Re is a function of size and settling velocity. The difference in drag coefficient is more significant for coarse and giant particles (approximately Re up to 10), where the drag coefficient given by (Clift and Gauvin, 1971) can be up to 2 times greater than that of Stokes. For this reason, we have decided to describe in detail how the new size-dependent drag coefficient is applied in our numerical experiments. We agree with the reviewer that in the initially submitted manuscript all these aspects were not clearly stated. Regardless, we have put an effort on reducing the length of the paragraph. The revised text (see lines 156-214, pages 6-8), is given below:

"In the GOCART-AFWA dust scheme of WRF, the forces acting on a dust particle moving along the vertical direction are the gravitational force F_g and the aerodynamic drag force F_{drag}, which are mathematically expressed in Eq.3 and Eq.4, respectively.

$$F_g = \rho_p \cdot V_p \cdot g, \quad (3)$$

$$F_{drag} = \frac{1}{2} \cdot \frac{C_D}{C_{cun}} \cdot A_p \cdot \rho_{air} \cdot u_{term}^2,$$

(4)

Where ρ_p stands for particle density in kgm^{-3}, g corresponds to the gravitational acceleration in ms^{-2}, $V_p = \frac{1}{6} \cdot \pi \cdot D_{eff}^3$ is the particle volume in m^3 and $A_p = \frac{\pi}{4} \cdot D_{eff}^2$, is the particle's projected area normal to the flow in m^2, ρ_{air} is the air density in kgm^{-3}. and D_{eff} represents the particles' diameter in m for each model size bin (assuming spherical particles, as defined in Sect. 2.1.1). C_D is the aerodynamic drag coefficient (unit less) and C_{cun} is the slip correction to account for slip boundary conditions (Davies, 1945) and it is expressed as a function of the air mean free path (λ, in meters) (Eq. 5):

$$C_{cun} = C_{cun}(\lambda) = 1.0 + \frac{2 \cdot \lambda}{D_{eff}} [1.257 + 0.4 \cdot e^{\frac{-1.1 \cdot D_{eff}}{2 \cdot \lambda}}],$$

(5)

The constant velocity that a particle builds up falling vertically within the Earth's atmosphere, is defined as the terminal settling velocity u_{term}, and it can be estimated by solving the 1-D equation of motion at the steady state limit, where net force is assumed to be equal to zero:

$$\rho_p \cdot V_p \cdot g = \frac{1}{2} \cdot \frac{C_D}{C_{cun}} \cdot A_p \cdot \rho_{air} \cdot u_{term}^2,$$

(6)

In the default GOCART-AFWA dust scheme the drag coefficient is given by Stokes' Law and is defined as:

$$C_D = \frac{12}{Re},$$

(7)

Where Re is the Reynold's number (unit less) given by the following equation as a function of the particle volume equivalent effective diameter D_{eff}:

$$Re = \frac{\rho_{air} \cdot u_{term} \cdot D_{eff}}{2 \cdot \mu},$$

(8)

Where μ is the air dynamic viscosity in $\frac{kg}{m \cdot s}$ defined as a function of air temperature T in K by the following equation (Hilsenrath, 1955; United States Committee on Extension to the Standard Atmosphere., 1976):

$$\mu = \frac{\beta \cdot T^{\frac{3}{2}}}{T+S}, \quad (9)$$

where S is the Sutherland constant which equal to 110.4 *K and* β *is a constant which equals to* $1.458 \cdot 10^{-6}\ kg \cdot m^{-1} \cdot s^{-1} \cdot K^{-1/2}$.

and the air mean free path is expressed as:

$$\lambda = \frac{1.1 \cdot 10^{-3} \cdot \sqrt{T}}{P} \quad (10)$$

Where T *is the air temperature in* K *and* P *the air pressure in* hPa.

The slip-corrected drag coefficient of the Stokes' Law ($\frac{12}{Re \cdot C_{cun}}$*) is valid only for Re <<1, thus it is not representative for particles with* D_{eff} *larger than ~10 μm. Therefore, an adaptation of the drag coefficient is needed in order to be valid for higher Re values (i.e., 0<Re<16), since in our work dust particles with diameters larger than 20 μm are considered. To realize, we use the drag coefficient* C'_D *(Eq. 11), proposed by Clift and Gauvin, (1971):*

$$C'_D = \frac{12}{Re} \cdot (1 + 0.2415 \cdot Re^{0.687}) + \frac{0.42}{1+\frac{19019}{Re^{1.16}}},\ for\ \ Re < 10^5 \quad (11)$$

Mallios et al., (2020) used the same C'_D *as a reference for the development of a drag coefficient for prolate ellipsoids, as more suitable for* $Re < 10^5$. *The departures between the drag coefficients given by Stokes and Clift and Gauvin (1971) become more evident for increasing particles' sizes. More specifically, the drag coefficient given by Clift and Gauvin (1971) can be up to 2 times higher than those of the Stokes' Law for coarse and giant particles (Fig. S1).*

In the default WRF code the slip correction is applied unconditionally for all the Re values, probably without affecting the solution significantly due to the small particle sizes ($D_{eff} < 20\ \mu m$*). However, in our work required a condition is required for applying the slip correction only in the Stokes' regime (e.g. Re < 0.1, Mallios et. al, 2020). Hence, we apply the bisection method to calculate the terminal velocity for each model size bin using the revised drag coefficient and, at first, ignoring the slip correction. When the solution lies in the Stokes' regime (e.g. Re < 0.1), we recalculate the settling velocity using the corrected drag coefficient* $C'_{D,slip} = \frac{C'_D}{C'_{cun}}$ *, where* $C'_{cun} = C_{cun}(\lambda')$ *with* λ' *the mean free path obtained by (Jennings, 1988):*

$$\lambda' = \sqrt{\frac{\pi}{8}} \cdot \frac{\frac{\mu}{0.4987445}}{\sqrt{P\rho_{air}}}, \quad (12)$$

“

Nevertheless, according to the reviewer’s suggestion, we included a plot in the supplement, which shows a comparison between the drag coefficients given by Stokes and Clift and Gauvin (1971) along with its relevant difference with respect to the Reynolds number Re. The comparison in Fig. R1 shows that the drag coefficient by Clift and Gauvin (1971) can be 2 times higher than Stoke’s drag coefficient, for Re up to 1, suggesting the necessity of the implementation of the revised drag coefficient. Figure R1 is also included in the Supplementary material (denoted as Fig.S1).

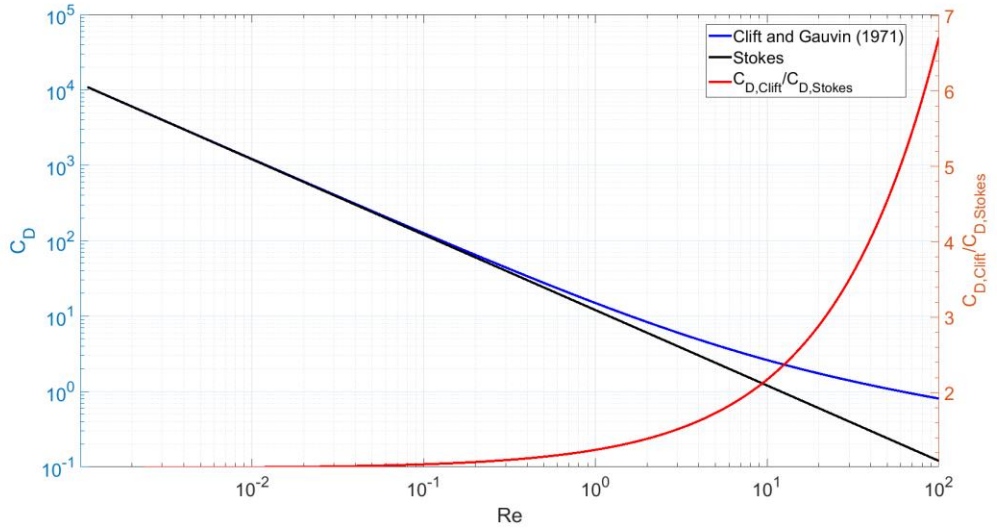

Figure R1: Drag coefficient for spheres given by the Stoke’s approximation (black line) and the expression proposed by Clift and Gauvin (1971) (blue line). The red line represents the relative difference between the two drag coefficients.

Finally, we included a comment, related to the drag coefficient differences, in the revised document in line 204, page 7:

“The departures between the drag coefficients given by Stokes theory and Clift and Gauvin (1971) become more evident for increasing particles’ sizes. More specifically, the drag coefficient given by Clift and Gauvin (1971) can be up to 2 times higher than those of the Stokes’ Law for coarse and giant particles (Fig. S1).”

- **This paper was posted online a few days before the publication of a rather similar paper by Meng et al. in GRL that also found that the settling speed needs to be greatly reduced for a large-scale model to match measurements of coarse and giant dust particles. A brief comparison between the results in the two papers should be included.**

We totally agree. Therefore, a comparison between our results and those of Meng et al. 2022 is included in the Discussion section of the revised manuscript. We performed a short analysis of the differences in the settling velocities between the different scenarios hypothesized in the two surveys.

In our work, we reduced the settling by 20, 40, 60 and 80 per cent and found that a 60-80% reduction is needed to match the model with observations of giant and coarse particles in the vicinity of Cape Verde. In Meng et al. (2022), the authors, after reducing the settling velocity by 13% (UR13) for accounting for particles' asphericity based on Huang et al., (2020), performed sensitivity tests where they replace particle density (2500 kgm^{-3}) with lower values and found that a decrease in the modeled dust aerosol density by a factor of 10-20 ($\frac{\rho_D}{10}$ or $\frac{\rho_D}{20}$), after accounting asphericity, is needed to improve the comparison between model and long-range dust observations of coarse particles. Despite the differences between the two works, especially in the calculation of the particles settling velocities (the two studies utilize different drag coefficients), the PSD which is used for the distribution of the emitted dust in the transport bins (the PSD in the Drakaki et al., (2022) parameterization is coarser for diameters greater than ~10 μm with respect to "observed FENNEC-PSD", Fig. R2) and the model spatial resolution (Meng et. al, (2022) uses the Comunity Earth System Model version 1.2 (CESM-v1.2) with the Community Atmosphere Model version 4.0 (CAM4) with 210 km x 277 km grid spacing, while in this study we use the WRF-Chem version 4.2.1 with the GOCART AFWA dust scheme with

15km x 15km grid spacing), both studies are suggesting a reduction in the settling velocity of the same order of magnitude. Fig. 5 shows a comparison of the different scenarios included in the two studies. The corresponding calculations have been performed assuming US Standard Atmosphere conditions. A reduction of particle density reduced by a factor of 10 (starting from the Clift and Gauvin (1971) drag coefficients) is almost equivalent to a decrease of 90% in the settling velocities. It is clear that a huge reduction in the settling velocity in both the Meng et al., (2022) methodology and this work is required, although the physical processes occurring to explain this reduction are not clear.

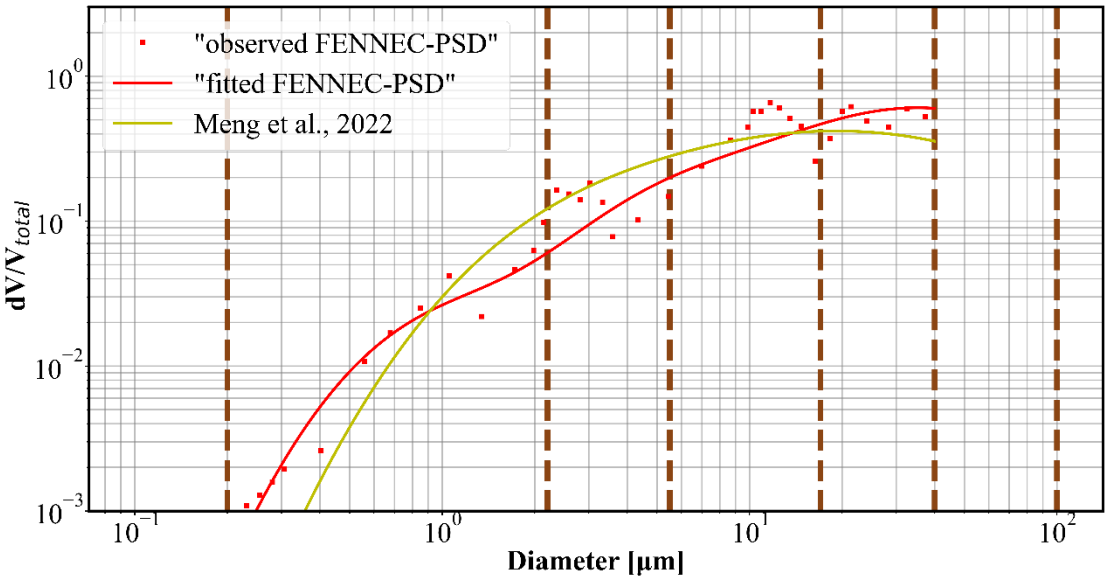

Figure R2: Comparison of the "fitted FENNEC-PSD" (red line) which is used in the dust parameterization in WRF-L and the PSD of the extended brittle fragmentation theory presented in Meng et. al., (2022) (yellow line). Red squares provide the "observed FENNEC-PSD" All volume size distributions are normalized in order to yield unity for the total volume of particles with diameters between 0.1 and 40 μm.

Figure R2 above shows the PSDs that have been utilized in the studies: Meng et al., (2022) in yellow and that in this study in blue. The black dashed line indicates the observed FENNEC-PSD (at 1km) as presented in Fig2a of the revised manuscript. All volume size

distributions are normalized in order to yield unity for the total volume of particles with diameters between 0.1 and 40 μm.

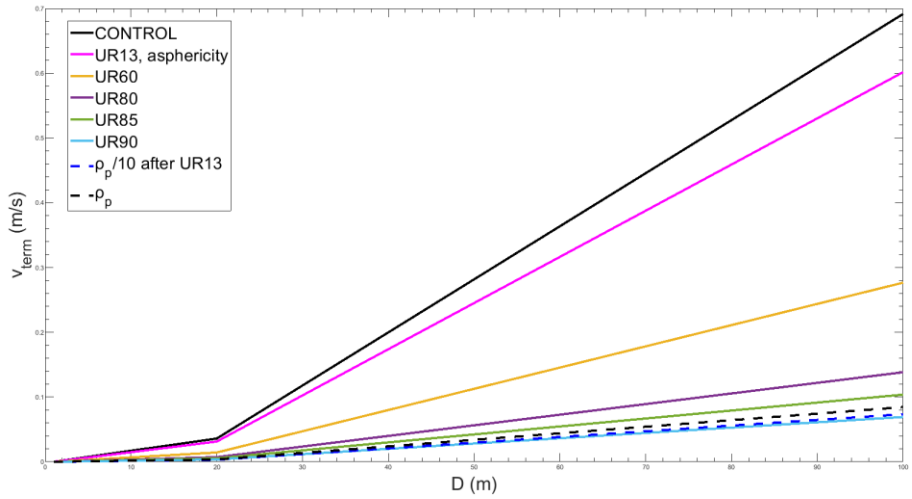

Figure R3: Terminal settling velocities with respect to particle diameter for dust particles, starting from the drag coefficient of Clift and Gauvin, (1971) and for the different scenarios described in Table R1.

Figure R3 above shows the terminal settling velocities with respect to particle diameter for dust particles, starting from the drag coefficient of Clift and Gauvin (1971) and for the different scenarios described in Table R1 below.

Table R1: Different numerical experiments presented in Fig. S5

Cases	Description
UR60	**settling velocity reduced by 60%**
UR80	**settling velocity reduced by 80%**
UR13	**settling velocity reduced by 13%**
ρD/10	**particle densities reduced by a factor of 10**
UR13&ρD/10	**particle densities reduced by a factor of 10 and settling velocity reduced by 13%**
UR85	settling velocity reduced by 85%
UR90	settling velocity reduced by 90%

Based on our reply we added a part in the Discussion section where we discuss the comparison between the two studies (see

lines 451-458, page 15). We also added Fig. R3 and Table R1 in the supplementary material, as Fig. S5 and Table S1 respectively.

"Meng et al. (2022) performed a similar study, where after reducing the settling velocity by 13% for accounting for particles' asphericity based on Huang et al., (2020), they performed sensitivity tests reducing the dust particles' density from 2500 kg m^{-3} to 1000, 500, 250 and 125 kg m^{-3}. They found that a decrease in the modelled dust aerosol density by 10-20 times its physical value (i.e., from 2500 kg $m^{-3}$to 250-125 kg m^{-}3) is needed to improve the comparison between the model and the long-range dust observations of coarse particles. A 10 times reduction in particles' density is almost equal to a 90% reduction in the settling velocity (starting from the Clift and Gauvin (1971) drag coefficients and assuming conditions of U.S. Standard Atmosphere, Fig S5). It is clear that a huge reduction in the settling velocity in both the Meng et al., (2022) methodology and this work is required, although the physical processes occurring to explain this reduction are not clear."

- **Lines 135-140 and Fig. 2: Here and elsewhere in the paper (section 2.2.2, Figure 5), not enough detail is provided on the used in situ measurements. Please describe exactly which runs were used for this data, how measurements were averaged over different runs and any other processing. Which instruments of the FENNEC and AER-D data did you use and how did you treat data that overlapped in the particle size range? And please include the measurement uncertainties and describe what's included in them.**

We agree with the reviewer that we have to clarify more the aspects relating to the measurements used in this work, the specific instrumentation and their corresponding errors. Regarding the PSD we use to modify the parameterization of emitted dust and calculate the dust fraction of emission for each size bin ($k\_factors$), we use size distributions from the Fennec field campaign from aircraft profiles over the Sahara (Mauritania and Mali) as described in Ryder et al. (2013). We select size distributions from"freshly uplifted dust" cases where dust is in the atmosphere for less than 12 h. Additionally, from these profiles we use data from the lowest available altitude, centered

at 1 km, covering altitudes between 750 m to 1250m. This is depicted by the red squares in Fig.2(a), hereafter referred to as the 'observed FENNEC-PSD'. Error bars in Fig 2a indicate the standard deviation across the profiles and altitudes contributing to this data. The instrumentation for those measurements was the Passive Cavity Aerosol Spectrometer Probe (PCASP, 0.13-3.5 μm), the Cloud Droplet Probe (CDP, 2.9-44.6 μm), using light scattering measurements and assuming a refractive index (RI) of 1.53-0.001i (which is constant with particle size), spherical shape for the particles, and using Mie calculations to convert from optical to geometric diameter, as well as the Cloud Imaging Probe (CIP15, 37.5-300 μm)). The instruments and data processing are described in Ryder et al. (2013a). The midpoint size bin diameters do not overlap, though there is some overlap in bin edges between the instruments. A fit on the observations is provided in Fig.2a (the "fitted FENNEC-PSD" with solid red line).

Regarding the PSDs of the AER-D campaign, we used in-situ observations during horizontal flight legs at a constant height (refered as RUNs or flight segments) over the Atlantic Ocean during AER-D. We used measurements taken with PCASP (D =0.12-3.02 μm) for fine dust particles. For the coarse and giant mode of dust we used measurements from CDP (D=3.4-20 μm, although CDP measurements availability extends up to 95.5 μm as explained below) and the two-dimension Stereo probe (2DS, D = 10–100 μm - although the instrument measures up to 1280 μm few particles larger than 100μm were detected). For the light scattering techniques of PCASP and CDP, a RI = 1.53-0.001i is assumed for the conversion of the optical to geometric diameter (as in FENNEC 2011 campaign). CDP observations extend up to the size of 95.5 μm, thus data from CDP and 2DS partly overlap in their size range. Since 2DS observations are more reliable in the overlapping size range, we used

the CDP observations for particles with sizes up to 20 μm. Also, 2DS-XY observations are preferred over the 2DS-CC, since they better represent the non-spherical particles. A more detailed description of the in-situ instruments and the corresponding processing of the data acquired during the AER-D campaign is included in Ryder et al., (2018). The errors in the AER-D PSDs are the total errors (random and systematic, see Ryder et al., (2018)). All PSD measurements are at ambient atmospheric conditions. The locations of the flights of AER-D used in this study are depicted in Fig.3.

Based on our reply we have revised the parts in the original manuscript in Sect. 2.1.1 (Lines141-148, page 5):

"We rely on prescribed PSD for the emitted dust particles at the source based on the airborne in situ measurements acquired during the FENNEC campaign of 2011 (Ryder et al., 2013a). More specifically, for the freshly uplifted dust we use the mean PSD at the lowest available height (i.e., 1km) t, obtained by averaging profile measurements above the Sahara (Mauritania and Mali), hereafter called the "observed FENNEC-PSD", which is shown in Fig. 2(a) with red squares. Figure 2a shows also the "fitted FENNEC-PSD" (solid red line), which is the fit of the "observed FENNEC-PSD", using five lognormal modes (Table 4). In Sect. 2.2.1 more information is provided on the derivation of the mean "observed FENNEC-PSD", including also the description of the FENNEC 2011 campaign, the in-situ instrumentation used and the processing of the acquired data."

And in 2.2.1 Section (Lines 278-306, pages 10-11):

"During the FENNEC field campaign in 2011 (Ryder et al., 2013b, 2013a) and the AER-D field campaign in 2015 (Ryder et al., 2018, 2019), airborne in situ observations were collected with the FAAM BAE research aircraft.

In this study we use size distributions from the FENNEC field campaign, aquired during aircraft profiles over the Sahara (Mauritania and Mali), as described in Ryder et al. (2013a). We select size distributions from "freshly uplifted dust" cases, when dust particles are in the atmosphere for less than 12 h. Additionally, from these profiles we use data from the lowest available altitude, centered at 1km, covering altitudes between 0.75 to 1.25km. The derived PSD is depicted in Fig.2(a), hereafter referred to as the "observed FENNEC-PSD". Error bars in Fig.2(a) indicate the standard deviation of the observed values across the profiles and altitudes we used. The instrumentation for those measurements was the Passive Cavity Aerosol Spectrometer Probe (PCASP, 0.13-3.5 μm), the Cloud Droplet Probe (CDP, 2.9-44.6 μm), using light scattering measurements and assuming a refractive index (RI) of 1.53-0.001i (which is constant with particle size), spherical shape for the particles, and using Mie calculations to convert from optical to geometric diameter, as well as the Cloud Imaging Probe (CIP15, 37.5-300

μm)). The instruments and data processing are described in Ryder et al. (2013a). The midpoint size bin diameters do not overlap, though there is some overlap in bin edges between the instruments. A fit on the observations is provided in Figure 2a (the "fitted FENNEC-PSD" with solid red line), which is used in the parameterization of the emitted dust, as described in Section 2.1.1, to modify the GOCART-AFWA dust scheme in WRF.

We also use PSD observations during horizontal flight legs at a constant height (referred either as RUNs or flight segments) over the Atlantic Ocean during AER-D. We use measurements taken with PCASP (D =0.12-3.02 μm) for fine dust particles. For the coarse and giant mode of dust we used measurements from CDP (D=3.4-20 μm, although CDP measurements availability extends up to 95.5 μm as it is explained below) and the two-dimension Stereo probe (2DS, D = 10–100 μm -although the instrument measures up to 1280 μm few particles larger than 100μm were detected). For the light scattering techniques of PCASP and CDP, a RI = 1.53-0.001i is assumed for the conversion of the optical to geometric diameter (as in FENNEC 2011 campaign). CDP observations extend up to the size of 95.5 μm, thus data from CDP and 2DS partly overlap in their size range. Since 2DS observations are more reliable in the overlapping size range, we used the CDP observations for particles with sizes up to 20 μm. Also, 2DS-XY observations are preferred over the 2DS-CC, since they better represent the non-spherical particles. A more detailed description of the in-situ instruments and the corresponding processing of the data acquired during the AER-D campaign is included in Ryder et al., (2018). The error bars represent the total (random and systematic) measurement error due to the counting error, the discretization error, the uncertainties in the sample area and the uncertainties in the bin size due to Mie singularites (Ryder et al., 2018). All PSD measurements are at ambient atmospheric conditions. The locations of the flights of AER-D used in this study are depicted in Fig.3."

- **240-241: "The fine resolution increases the accuracy of the dust simulations and provides a good estimate of the missing mechanism." Please include either citations or original results that support this statement. Also, how does the fine resolution affect the numerical diffusion in the model? And please include a discussion in this section of the numerical diffusion in WRF-Chem as Ginoux (2003) hypothesized this to be a main factor in why coarse dust particles deposit too quickly in models. Currently, there's only a brief mention of this in the last paragraph of the paper but not really any discussion of how big a problem numerical diffusion is in WRF-Chem and thus of whether it can explain your results.**

The resolution applied here is adequate for the scale of phenomena we want to study. With the term ”fine resolution” we wanted to denote that we have a finer resolution with respect to global datasets (e.g. 0.5 deg GFS), which will fail to reproduce the appropriate weather fields and dust fields (Cowie et al., 2015; Basart et al., 2016; Roberts et al., 2017; Solomos et al., 2018). However, the reviewer is correct that this can be misleading so we made changes in the original manuscript (lines 235-238, page 8).

“The resolution applied in this study (15km grid spacing) is adequate for the scale of phenomena we want to study, improves the representation of topography and increases the accuracy of the reproduced weather and dust fields, compared to coarser resolution, such as used in global datasets (e.g. 0.5 deg GFS) (Cowie et al., 2015; Basart et al., 2016; Roberts et al., 2017; Solomos et al., 2018).”

The WRF-Chem uses a spatially 5th-order horizontal advection and a 3-rd order vertical advection in the scalar conservation equation coupled with the 3-rd order Runge-Kutta time integration schemes which are non-diffusive schemes. Moreover, WRF-Chem uses the first order explicit advective scheme for the scalar concentration in the equation of gravitational settling. The first-order upstream scheme is notoriously too diffusive. Since the numerical diffusion is pointed out in Ginoux (2003) as a possible source of the model underestimation of dust coarse particles, the use of a less diffusive scheme in WRF settling parameterization could improve the accuracy of modelled dust concentration fields. Based on our reply we have added a discussion about numerical diffusion in WRF-Chem in Section 2.1.3 (page 238-244, line 8-9)

“WRF-Chem solver uses a 5th-order horizontal advection scheme and a 3-rd order vertical advection scheme to solve the scalar conservation equation, along with the 3-rd order Runge-Kutta time integration scheme (Grell et al., 2005). The use of such high-order advective schemes eliminate the numerical errors of diffusion in the code. We should note though that in the deposition parameterization of GOCART-AFWA dust scheme the vertical advection of the losses due to the gravitational settling is solved by a first order explicit scheme, which is notoriously too diffusive (Versteeg and Malalasekera, 2007) and thus it can possibly induce numerical errors in the mass conservation (Ginoux, 2003)”

- **Section 2.1.4: here the effect of asphericity on dust extinction is neglected, which could be substantial. I think that's fine as the focus is on the size distribution, but please note that simplification.**

Although we agree with the reviewer that the effect of the asphericity may be substantial, there is no available data (to our knowledge) of the extinction coefficient of dust particles with realistic irregular shapes. The commonly-used spheroidal shapes do not provide substantial differences for the extinction coefficient of the particles, at least when considering the aspect ratios measured for dust particles in Sahara (as these are provided by Kandler et al. (2009), as shown in Tsekeri et al. (2022). We have included the above in Section 2.1.4 in lines 255-273 and page 9:

"Although the extinction coefficient values for spherical particles may be different from the extinction coefficient values of the dust particles, which have irregular shapes, to our knowledge there is no data available for the extinction coefficient of the latter. The extinction coefficient values of spheroidal shapes, commonly used as a proxy of the dust shapes, are not substantially different compared to the spherical particles (Tsekeri et al., 2022), at least when considering the aspect ratios measured for dust particles in Sahara (Kandler et al., 2009)."

- **(16): here the units for dust mass concentration, particle density, and diameter don't match (they all use different length scales). Please correct.**

We would like to thank the reviewer for pointing this out. After the revision of the document the right equation is :

$$DOD_{550,n} = \sum_1^k \frac{3}{2\rho_{,k} D_{eff,k}} ML_{n,k} Q_{ext550,k}, \quad (14)$$

Where $ML_{n,k}$ is the columnar dust load in g/m^2 for each grid box n and for each model size bin k.

However, based on RC3 we removed the related part from Section 2.1.4.

- **Line 273: please elaborate on how you are "taking into account the absolute difference between WRF forecast time and Aqua overpass time"**

In the model, the DOD is computed in each grid model box and its instantaneous value is provided every one hour. The DOD value from Aqua satellite is acquired from the ModIs Dust AeroSol (MIDAS) DOD product, based on the following spatiotemporal collocation procedure: First, we reproject the model DODs on an equal lat-long grid at 0.4° x 0.4° spatial spacing. We should note that the model DOD field has no spatial gaps and is provided instantaneously for every hour. The MIDAS DOD is available in swath level (5-minute segments, viewing width of 2330 km) along the MODIS-Aqua polar orbit. Then, the two closest WRF outputs to the Aqua satellite overpass time are used to calculate a weighted-average WRF-DOD, by taking into account the temporal departure between forecast and overpass times, only for the WRF grid cell that coincides with the observations. Please note that we have removed the corresponding part related to b920 flight, based on RC3 comment.

I find Figure 5 hard to interpret and I think a lot more information is needed here. The text notes (L. 347) that this result is for "an emission point in Mali" - could you indicate exactly what location? And are the model results here for the closest grid box? Did the model include emissions only from that grid box or from the entire domain? And see comments above on more details needed for the experimental data. Is this the same data as shown in Fig. 2a, except sorted into the five bins? And could you also include uncertainties on the measurements? I also recommend including your parameterized size distribution at emission to help interpret the model results.

In Figure 5 we present the change of the PSD with height above an emission point in Mali, on 11/08/2015 at 14UTC. At this particular

time, a dust emission was initiated, with the maximum intensity for the broader area of Mali at the model grid point with altitude=24.9◦ and longitude=9.2◦. The model PSDs in Figure 5 are from that grid box, after interpolating the model PSDs at 1, 2 and 3 km height. The red squares in Figure 5 correspond to the "observed FENNEC-PSD" (mean PSD of freshly uplifted dust cases at 1km) sorted into the five bins and the corresponding error bars indicate the maximum and minimum limits of the "observed FENNEC-PSD", sorted into the five model size bins, after including the standard deviation of "observed FENNEC-PSD". The black squares depict the "fitted FENNEC-PSD" sorted into five bins, which are used in the model parameterization to distribute the emitted dust mass into the five model bins. We agree with the reviewer that the description was incomplete and we have inserted additional information in the part of the discussion of Figure 5 in Sect 3.2 of the revised manuscript. Based on that and other reviewer comments we modify the Section 3.2 (see lines 334-359, page 12):

"In Fig. 5 we present how the PSD varies with height above an emission point (latitude=24.9º and longitude=9.2º) in Mali, on 11/08/2015 at 14UTC. The model PSDs are only from that grid model box interpolated at 1, 2, and 3 km height and for the particular timestep (11/08/2015 at 14UTC). The red squares correspond to the "observed FENNEC-PSD" sorted into the five bins. The error bars provide the maximum and minimum limits of the "observed FENNEC-PSD", sorted into the five model size bins, after including the standard deviation of "observed FENNEC-PSD". The "observed FENNEC-PSD" (see Section 2.2.1) has been derived from several flights above dust sources, thus it is representative of the PSDs above Sahara sources and it used here as reference. The black squares depict the "fitted FENNEC-PSD" sorted into five bins, used in the model parameterization to calculate the emitted dust mass of the corresponding five model transport bins. The difference between the "fitted FENNEC-PSD" and the "fitted FENNEC-PSD" occurs due to the fitting process. The modelled volume concentration is reduced with height by an order of magnitude between 2 and 3 km for particles with diameters 17-40 μm (bin 4). At 3km the simulated concentrations of particles in bin 4 and bin 5 are very low compared to the measurements in Fig. S2a of Ryder et al., (2013a) which indicate the removal of giant particles above 4 km (Ryder et al., 2013a, Figure S2a). Although a direct comparison between the modelled and the observed PSD for this particular emission point is not feasible, since the FENNEC campaign took place on different dates than the AER-D and there are no available measurements above dust sources for the period we performed our simulations, we note a modification of the PSD shape, both

for model and observations at 1km. It is evident that the model overestimates the PSD for bins 1-3 while the opposite is found in the size spectrum of the super-coarse (bin4) and giant (bin5) dust particles. Therefore, a model weakness is revealed at the very early phase of the dust transport. Those differences can be attributed to an overestimation of their loss during uplift from the surface to 1 km, or to higher updrafts that remain unresolved in our numerical experiment. Another possible source of this underestimation could be the utilization of a not well-defined PSD shape constraining the distribution of emitted dust mass to the model transport size bins. The use of a PSD with a higher contribution of coarse and giant dust particles could possibly improve the representation of the coarse and giant particles aloft (Fig. S2 and S3) and can be assessed in future studies. Additionally, comparing the "observed FENNEC-PSD" with the modelled PSD of the scenario with the maximum relative reduction of the settling velocities (UR80) in Fig. 5, we find a significant increase of the modelled volume concentrations, reducing the differences seen in volume concentrations in bin4 and bin5 without the reduction of the settling velocity, although the underestimation in bin 5 is still evident."

Moreover, we plot again Figure 5 after other reviewers' recommendations, adding the observed mean PSD of "freshly uplifted dust" during Fennec 2011 in red squares ("observed FENNEC-PSD sorted in 5 bins") along with the standard deviation of the observed values within the size bin. The "fitted FENNEC-PSD sorted in 5 bins", which is used at the parameterization of the emission, is depicted with black squares in the revised plot. Here we must note that the label in the legend "observations" was not correct, since, in Figure 5 of the original, the red squares corresponded to the "fitted FENNEC-PSD" instead. We corrected the legend accordingly. The revised figure is inserted in the revised document in lines 915-922 and page 34

"

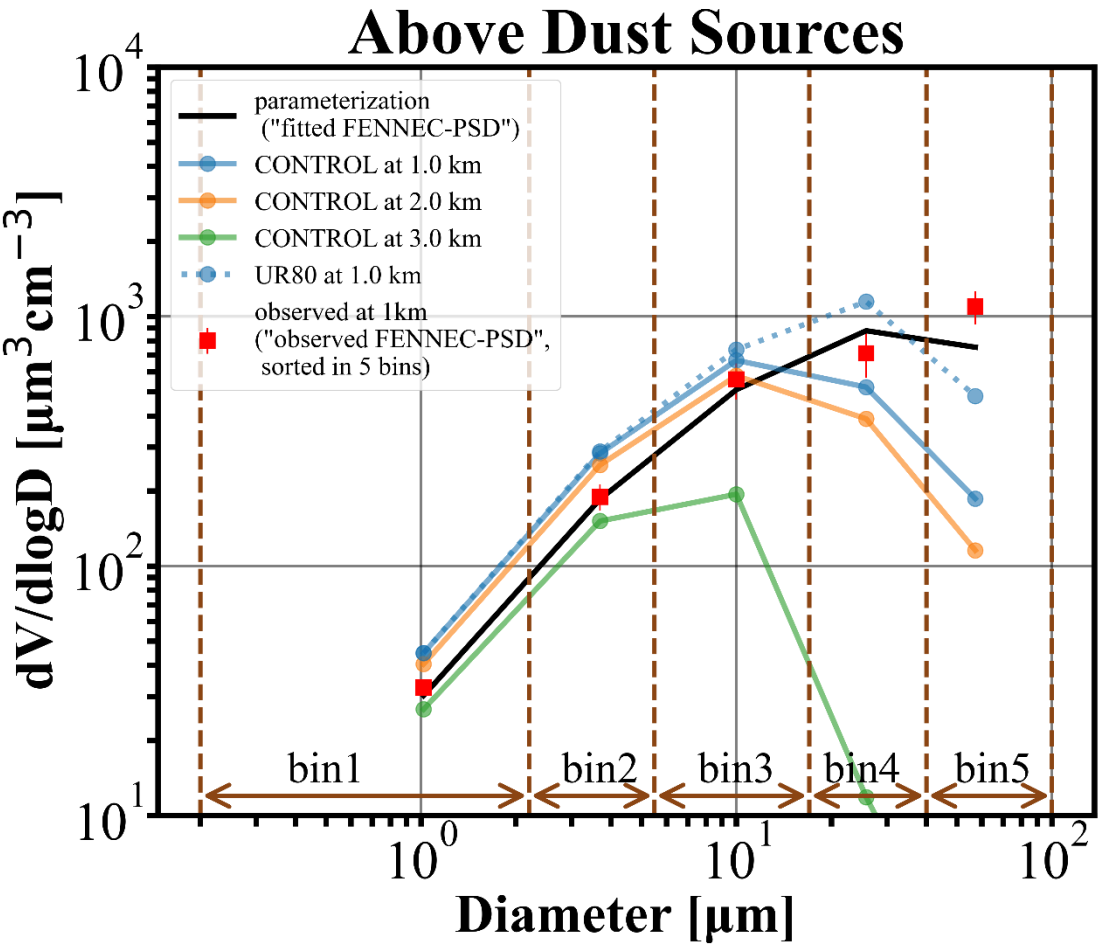

Figure 5: Dust size distribution above an emission model grid point (latitude=24.9° and longitude=9.2°) in Mali, on 11/08/2015 at 14UTC. Blue solid line: the modelled dust PSD of the CONTROL run interpolated at 1 km altitude above the dust source, orange solid line: the modelled dust PSD of the CONTROL run interpolated at 2 km altitude above dust source, green solid line: the modelled dust PSD of the CONTROL run interpolated at 3 km altitude above dust source, blue dotted line: the modelled dust PSD of the UR80 run interpolated at 1 km altitude above the dust source and red squares: the "observed FENNEC-PSD" sorted in 5 bins (observed at 1 km altitude), black squares: the "fitted FENNEC-PSD" sorted in 5 bins which has been used for the distribution of the model emission to the five size bins used in the model."

- **L377-380: Why do you average over the eight neighbouring grid points when you're already interpolating the measurements? Some more explanation is needed here.**

We agree with the reviewer that we should explain more the way that model results are collocated to the AER-D measurements. In the collocation procedure, we firstly interpolate the model dust fields to the specific height of each flight leg (or "RUN"). Afterwards, we find the closest grid box to the flight leg coordinates and its eight neighbouring grid boxes in the same level height. The selection of the model grid points is done from the two hourly model outputs that enclose the time of flight RUN. Finally, the dust field is averaged among the selected grid boxes and selected times and the variability is expressed in terms of the standard deviation. In case that the flight time coincides with the model output, we include in the averaging that particular hourly model output as well as the next and previous hours' outputs. Based on our reply, we updated the related parts in the revised manuscript in lines 374-383, page 13:

"The red squares correspond to the observations and the error bars denote the total (random and systematic) measurement error (see Sect 2.2.1). The modelled PSDs are collocated in space and time with the measurements of each flight segment. For each flight segment, we extract the modeled PSD by interpolating the dust field to the specific altitude of the flight RUN. Additionally, we average the dust field of the nearest grid cell to each coordinate pair along the flight segment track, and the eight neighbouring grid cells of the same altitude. The coordinates of the flight leg track are depicted with orange dots and the collocated grid points used for deriving the modelled PSD (at the specific height of each flight leg) with blue dots. In the time dimension, we average the two hourly model outputs that contain the times of the measurement. In case that the time of measurement coincides with the exact hourly output, the model output on that hour along with the outputs prior and after that are averaged. The error bars in the model PSDs indicate the standard deviation of the collocated grid points averaging in space and time."

- **Figure 8: Please describe what exactly the error bars represent. Is this derived from the counting uncertainty in a given run? Or the standard deviation (or standard error?) over several measurements?**

We agree with the reviewer that we have to provide more information about the uncertainties of the measurements. The error bars in Fig. 7 (Fig 8 in the original manuscript) correspond to the total

measurement errors (random and systematic) due to the counting error, the discretization error, the uncertainties in the sample area and the uncertainties in the bin size due to Mie singularities (Ryder et al., 2018). Therefore, we modified the revised manuscript including a description in the caption of Figure 7 in lines 928-933, p 36:

"***Figure 7: Modeled and observed dust PSD of flight b928, over the Atlantic Ocean during AER-D, for straight-level-runs (a) R02, (b) R03, (c) R05, (d) R06, (e) R10, (f) R11 and (g) R12. The in situ observations are shown with red squares (along with the total measurement error). The collocated modeled PSDs are shown with lines, for the CONTROL run (black), UR20 (blue), UR40 (orange), UR60 (green), and UR80 (purple) and the corresponding standard deviation with the associated error bars. The brown vertical lines indicate the limits of the model size bins. The inlet maps show the flight segment track and the collocated model grid points.***"

We also modified Section 2.2.1 by adding the description of the error bars on the revised manuscript (page 10-11, lines 303-305):

"The error bars represent the total (random and systematic) measurement error due to the counting error, the discretization error, the uncertainties in the sample area and the uncertainties in the bin size due to Mie singularites (Ryder et al., 2018)."

We also modified Section 3.4 by adding the description of the error bars on the revised manuscript (page 13, lines 374-375):

"The red squares represent the observations and the error bars represent the total (random and systematic) measurement error (see Sect 2.2.1)."

- **Also for Figure 8: I find the results in Fig. 8a puzzling. The measurements shown here are at the very lowest level, only 38m above the ground. So presumably, these measurements were part of the data used in Fig. 2 to parameterize the emitted size distribution, is that correct? Then why does the model do so poorly in reproducing these measurements so close to the surface? Please show the emitted size distribution in this plot to help the reader interpret your model results. Please also discuss why the model does not capture the measurements so close to the**

ground, where errors in deposition would presumably have not as much impact on the results.

The observations depicted in Figure 7 (Figure 8 in the original manuscript) have been derived from the AER-D campaign, in the downwind area, over the Eastern Atlantic Ocean far from the dust sources. Thus, those observations contain the effects of dust deposition and dust transport. None AER-D data have been used for the model parameterization (only data from the FENNEC campaign have been used for the model parameterization, as described in Sections 2.1.1). The fact that the model underestimates the presence of the coarse and giant particles confirms that there is one or more physical mechanisms of the dust transport that the model misses or underrepresents. Obviously, this is not clear enough in the original manuscript, thus we add some text lines in Section 3.4 of the revised document (lines 370-374, p.13) noticing that issue:

"Figure 7 illustrates the simulated PSDs from each experiment (i.e., CONTROL and URx), along with those acquired by the airborne in situ measurements at different segments and altitudes of the flight b928 in the surrounding area of Cape Verde (downwind region). For the other AER-D flights (i.e., b920, b924, b932 and b934) similar findings are drawn and for brevity reasons are omitted here and are included in the supplementary material (Fig.S4). All AER-D measurements demonstrate the impacts of the processes that are associated with dust transport."

- **Figure 10: What are the gray, yellow, and blue shading here?**

  The shaded areas correspond to altitude ranges within the atmosphere. In order to simplify the plots in Figure 9a (Figure 10a in the original manuscript) and make both plots (a and b) more consistent with each other, we choose to remove the shading from Figure 9a. Below is the revised Figure 10a:

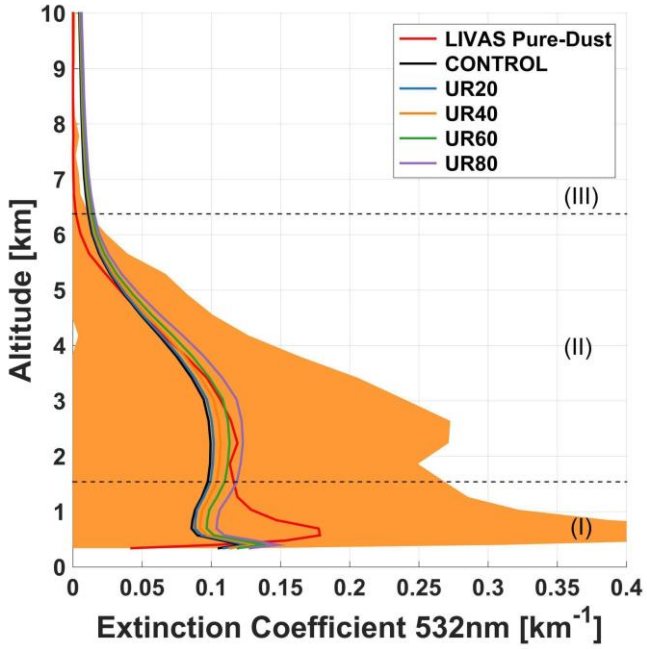

Also, in the revised Fig. 9 (Figure 10 in the original manuscript), based on other reviewers' suggestion, we included a figure showing the daytime and nighttime overpasses of CALIPSO. The revised Fig.9 is inserted in lines 947-955, page 38 of the revised manuscript:

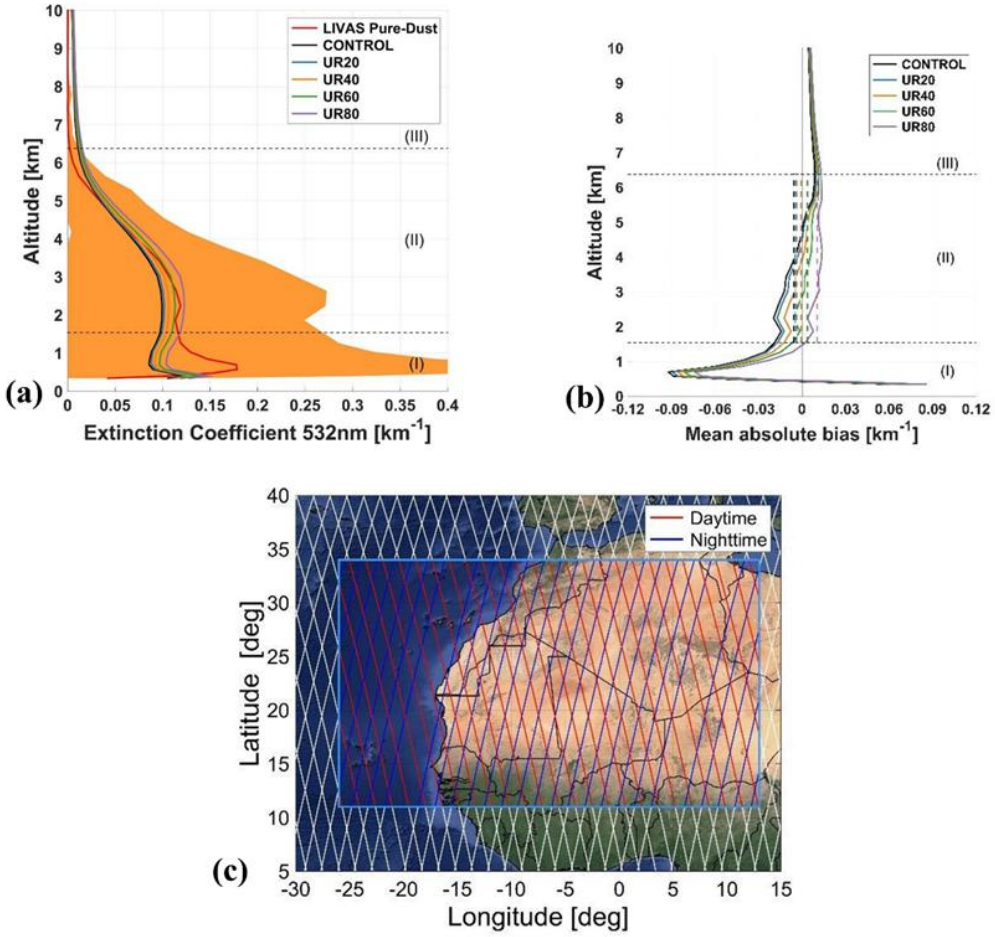

"Figure 9: (a) Profile of the mean extinction coefficient at 532 nm, by LIVAS pure-dust product (black red line), and profiles of the mean extinction coefficient at 532 nm simulated from the different experiments of Table 3 (CONTROL, UR20/40/60/80). The orange shading indicates the standard deviation of the LIVAS profile averaging. (b) The mean absolute biases between the LIVAS profile and the simulated profiles from the different experiments, in the domain of interest, between 05/08/2015 and 25/08/2015. The vertical dashed lines are the mean absolute bias between the LIVAS profile and the simulated profiles from the different experiments averaged over the altitudes of region II. (c) The domain of interest and the daytime (red) and nighttime (blue) CALIPSO overpasses. The vertical dashed lines are the mean absolute bias between the LIVAS profile and the simulated profiles from the different experiments averaged over the altitudes of region II."

- **Discussion and conclusion section: As written, this is really only a discussion section. I recommend the authors add a summary of the results of their study for the reader.**

We would like to thank the reviewer for the suggestion which will improve the structure and the presentation of our work. Below is the part of the Summary and conclusions in lines 504-546, page 17-18:

"In the current state-of-the-art atmospheric dust models, several physical processes governing dust life cycle components are not well represented or they are not included in the relevant parameterization schemes. This drawback, along with the lack of knowledge on the underlying mechanisms, results in the failure of the numerical simulations to reproduce adequately the long-range transport of super-coarse and giant mineral particles, as it has been justified via their evaluation versus sophisticated dust observations. The model limitations are well documented in literature, with one of the more critical to be the neglect of mineral particles with diameters larger than 20 μm, under the erroneous assumption that they deposit quickly after their emission.

In the current study, we modify the transport particle size distribution in WRF, expanding at size ranges up to 100 μm in diameter, by constraining the shape of the modelled PSD with the observed PSD from airborne in-situ measurements above dust sources, acquired in the framework of the FENNEC 2011 campaign. A novelty of our work constitutes the upgrade of the drag coefficient, determining the settling velocity of dust particles, accounting for realistic dust particles sizes ($Re < 10^{5}$), contrary to what is assumed in the traditional Stokes' theory. After optimally tuning the CONTROL run, we performed a series of sensitivity experiments in which the settling velocity has been reduced, aiming to artificially resemble the real forces acting on particles moving vertically and counteract gravitational settling. Our period of interest spans from the 5th to the 25th August 2015, when the AER-D campaign took place in the surrounding area of Cape Verde, residing in the core of the "corridor" of the Saharan dust transport along the Tropical Atlantic Ocean. In our experiments, the simulation domain covers most of the Sahara Desert (encompassing the most active dust sources worldwide) and the eastern sector of the Tropical Atlantic Ocean (receiving large amounts of mineral particles from the nearby Saharan dust sources). The dust-related numerical outputs produced by the CONTROL and URx experiments (referring to the reduction of the settling velocity by 20%, 40%, 60% and 80%, as expressed by the term x) are evaluated against the LIVAS satellite datasets providing pure dust extinction vertical profiles, respectively. Nevertheless, special attention is given on the evaluation of the WRF-L PSD against airborne in-situ measurements acquired in the framework of the AER-D campaign.

Based on our results, in the CONTROL experiment, the model tends to underestimate the dust volume concentration of coarse and giant dust particles since the very early stage of dust transport, when the emitted mineral particles are uplifted at 1 km above the sources. The initial model underestimation becomes more pronounced compared to the observations acquired during AER-D, particularly for the super-coarse (bin 4, sizes from 17 to 40 μm) and giant dust particles (bin 5, sizes from 40 to 100 μm), in the vicinity of Cape Verde (i.e., downwind region). Our findings are in line with the already stated underestimation of coarse and giant dust particles' presence during their long range dust transport. Nevertheless, when we gradually reduce the settling velocity (URx runs) the model performance steadily improves. Overall, among the numerical experiments, the best match of the simulated and the observed PSDs is achieved for the UR80 scenario (i.e., reduction of the settling velocity by 80%), highlighting the

misrepresentation or the absence of forces within the model parameterization schemes, acting on dust particles and counteract gravitational settling. Through the case-by-case inspection, it is revealed that the UR60 and UR40 scenarios can also occasionally provide the optimum agreement between the modelled and the observed PSDs, thus highlighting the complexity of the real physical processes that regulate the settling velocity and suspension of the dust particles. From the evaluation of the vertically-resolved simulated dust extinction coefficient at 532nm against the corresponding measurements from the LIVAS dataset, it is revealed that for the UR40 run the differences between the model and the observations are minimized (oscillating around zero), whereas the UR80 run outperforms the other runs in reproducing the vertical structure of the dust layers within the Saharan Air Layer. Summarizing, our work demonstrated an innovative approach in order to overcome existing drawbacks of the atmospheric-dust models towards improving the simulations of dust transport along the Tropical Atlantic Ocean. There are several candidate mechanisms, along with inappropriate definition and treatment of mineral particles in the parameterization schemes, hampering models in reproducing adequately the observed dust patterns. Despite our encouraging results, there are many mandatory steps towards upgrading the current state-of-the-art atmospheric dust models in anticipation of an optimum assessment of the multifaceted role of dust aerosols within the Earth-Atmosphere system."

- **441: The gravitational force acts on the center of mass and thus does not create a torque. Perhaps you mean that the aerodynamic force creates a torque? Please correct.**

We would like to thank the reviewer for pointing this out. Indeed, we meant the aerodynamic force instead of the gravitational force. Please note that based on that and RC3 comments we have revised the Section of the discussion and the referring part is omitted.

- **438-455: This is an interesting discussion of the effects of shape and particle orientation on settling speed. It left me confused on a few points though. The text states that "prolate spheroids fall faster than their spherical counterparts" even though their surface area is larger. How is that possible as more surface area would create more drag? This conclusion is also opposite of results in, for instance, Ginoux (2003). Do you perhaps mean that for this statement to apply to the special case when the prolate spheroid is aligned with its longest axis in the vertical direction, such that its cross-sectional area is smallest? If**

not, wouldn’t the drag of the spheroid relative to an equal-volume sphere depend on the orientation, which itself is unknown as it depends on a variety of factors including the electric field (per Mallios et al. 2021)?

Obviously, the statement here needs more explanation to avoid any misunderstanding. In lines 445-448 of the original manuscript, we state that "prolate spheroids fall faster than their spherical counterparts of the same volume" without specifying the orientation because prolate spheroids fall faster than their spherical counterparts of the same volume regardless of particle’s orientation (Mallios et al., 2020). Then in the next sentence, we explain that this happens due to two reasons. One is the projected area (and not the surface area) that depends on the particle orientation, and the other is the drag coefficient which is shape and orientation dependent. We would like to emphasize that the resultant drag force is proportional to the product of projected area and drag coefficient. Mallios et al. (2020) have shown clearly, that in the case of spheres and prolate spheroids (in the aspect ratio range 1.4-2.4) of the same volume, prolate spheroids fall faster, because the product of drag coefficient time the projected area is always smaller in the case of the prolate spheroids.

Moreover, we would like to add that the use of the surface area of the particle in the interpretation of the drag force's behavior can be misleading in that case and should be avoided. A prolate spheroid with a given major axis and aspect ratio has a specific value of surface area, regardless of its orientation. On the other hand, the projected area of the particle changes with orientation, affecting the drag force and the particle’s settling velocity.

Finally, we would like to add that the statement "prolate spheroids fall faster than their spherical counterparts of the same volume" does not contradict the findings of Ginoux (2003), because they compared

prolate spheroids and spheres of the same cross section (in their Eq. 10 the equivalent diameter Dp is calculated as the diameter of a sphere with the same cross section of a randomly oriented prolate spheroid). For a more detailed explanation of this, please check our response to the reviewer's next comment.

- **Later in this same section you seem to state the opposite conclusion (L. 452-5), that prolate spheroids do fall slower than spheres. But I think here the difference is that you're comparing it to spheres of the same max dimension (rather than volume)? I think this is quite confusing to the reader and I recommend you focus on the comparison that could actually explain that particles settle slower than your model simulations predict. And these measurements are presumably for volume-equivalent spheres? Or are these optical diameters, so it depends on the particle index of refraction and the shape of real dust particles? That should also be discussed in section 2.2.1 for the discussion here to add value. In general, I think the discussion on the effects of asphericity on settling should be presented more clearly for the statement on L. 476 ("the particle asphericity seems to be a strong candidate for the suggested corrections") to make sense to the reader.**

We can understand the reviewer's confusion. Even today, there is not a definite answer to the question "which one does fall faster? A sphere or a prolate spheroid?". The reason is that there are many parameters that influence the comparison. Ginoux (2003) compared randomly-oriented prolate spheroids and spheres of the same cross section. They showed that although spheroids fall slower, the difference between spheres and spheroids is negligible for aspect ratio values less than 5.

Huang et al. (2020) compared randomly-oriented ellipsoids and spheres of the same volume. They showed that ellipsoids fall around 20% slower than spheres.

Mallios et al. (2020) compared prolate spheroids and spheres of the same maximum dimension, and of the same volume. Moreover they did not assume randomly-oriented particles, but particles of specific orientation (horizontal and vertical). They showed that the results of the comparison change when the maximum dimension or the volume-equivalent size is used in the comparison changes (maximum dimension or volume). Prolate spheroids fall slower than spheres of the same maximum dimension, regardless of orientation. On the other hand, prolate spheroids fall faster than spheres of the same volume, regardless of orientation. The comparison with in situ observations of the maximum dimension of particles is not so common, since most of the in situ measurements do not provide the sizing of the particles in terms of their maximum dimension, with some exceptions, as e.g. the observations shown in van der Does et al. (2016) of individual giant mineral particles (larger than 100 μm in maximum dimension).

Based on our reply to this and the previous reviewer's comment, we modified the effects of asphericity discussion in page 15-16, lines 461-480 of the revised document as:

"One of the processes proposed in the literature to explain the longer atmospheric lifetimes of large mineral dust particles is the particle asphericity. Ginoux (2003) compared randomly-oriented prolate spheroids and spheres of the same cross section. They showed that spheroids fall slightly slower than their spherical counterparts, with their difference being negligible for spheroids with aspect ratio values less than 5.

Huang et al. (2020) compared randomly-oriented ellipsoids and spheres of the same volume. They showed that ellipsoids fall around 20% slower than spheres.

Mallios et al. (2020) compared prolate spheroids and spheres of the same maximum dimension, and of the same volume. Moreover, they did not assume randomly-oriented particles, but particles of specific orientation (horizontal and vertical). They showed that the results of the comparison change when the maximum dimension or the volume-equivalent size is used in the comparison. Prolate spheroids, with

aspect ratio values in the range of 1.4-2.4, fall slower than spheres of the same maximum dimension, regardless of orientation, with the relative difference between the settling velocities reaching the value of 52%. On the other hand, prolate spheroids, in the same aspect ratio value range, fall faster than spheres of the same volume, regardless of orientation. The comparison with in situ observations of the maximum dimension of particles is not so common, since most of the in-situ measurements do not provide the sizing of the particles in terms of their maximum dimension, with some exceptions, as e.g. the observations shown in van der Does et al. (2016) of individual giant mineral particles (larger than 100 μm in maximum dimension).

All the above show that more work is needed for the definite and accurate quantification of the particle asphericity effect on their settling. Nevertheless, there are indications pointing that aspherical particles remain in the atmosphere longer, and that asphericity can be one of the reasons for the differences between the modelling results and the observations."

I think the author contribution sections require more detail. There are a large number of authors with only a generic description of their contributions, with only the descriptions for ED, VA, AT, EP, and AG more specific. I think the contributions of each individual author should probably be spelled out more.

Absolutely. We revised the related part in the revised document (line549-564, page18-19) as:

"Author Contributions: *ED, VA, and AT design the study; SM guided ED on the methodology for the replacement of the drag coefficient. AT provided useful assistance on the treatment of airborne observations. CR provided the data from the airborne in situ measurements and provided useful information about the instrumentation methods; ED developed the code, performed the simulations and analyzed the results. AG and CR consulted ED on the methodology of in situ and WRF datasets. VA, EM and EP provided the LIVAS dataset, lead the collocation methodology and helped on the interpretation of the results. ED plotted the model and observation data (apart from LIVAS). EP treated and plotted LIVAS data; ED wrote the manuscript draft; VA, AT, AG, EP, SM, CS, SS, EM, CR, DB and PK provided critical feedback and reviewed and edited the manuscript."*

Technical corrections:

- **Can you provide a reference for Eq. 10?**

Absolutely. In the revised manuscript Eq.10 became Eq.9. So, Eq.9 of the revised manuscript is an equation of dynamic viscosity μ, based on the kinetic theory and comes from the general expression of Sutherland's Law:

$$\mu = \mu_o \cdot \frac{\left(\frac{T}{T_o}\right)^{3/2} (T_o + S)}{(T + S)}$$

but its constants are based on experiments (United States Committee on Extension to the Standard Atmosphere., 1976;). S is the Sutherlands constant equals to $110.4\,K$ and β is a constant equals to $1.458 \cdot 10^{-6}\, kg \cdot m^{-1} \cdot s^{-1} \cdot K^{-1/2}$. The value of β corresponds to a reference air temperature (To) of 273.16 K and an air viscosity (μo) at To which is equal to $1.716 \cdot 10^{-5} kg \cdot m^{-1} \cdot s^{-1}$ (White, 2006; Hilsenrath, 1955). We should note that this equation is included also in the original parameterization of AFWA-GOCART in WRF model. Based on our reply we provided the references for Eq.9 according to the reviewer suggestion in page 7 and line 187-193

"*Where μ is the air dynamic viscosity in $\frac{kg}{m \cdot s}$ defined as a function of air temperature T in K by the following equation (Hilsenrath, 1955; United States Committee on Extension to the Standard Atmosphere., 1976):*

$$\mu = \frac{\beta \cdot T^{\frac{3}{2}}}{T+S}, \qquad (9)$$

where S is the Sutherland constant which equal to 110.4 K and β is a constant which equals to $1.458 \cdot 10^{-6}\, kg \cdot m^{-1} \cdot s^{-1} \cdot K^{-1/2}$."

- **138: "upwelling" is probably not the right word here**
  Done
- **184: "become is" à "becomes"**
  Done
- **Line 448: I think ellipsoids here should be spheroids**
  Done

References

Basart, S., Vendrell, L. and Baldasano, J. M.: High-resolution dust modelling over complex terrains in West Asia, Aeolian Res., 23, 37–50, doi:10.1016/j.aeolia.2016.09.005, 2016.

Cowie, S. M., Knippertz, P. and Marsham, J. H.: A climatology of dust emission events from Northern Africa using long-term surface observations, Atmos. Chem. Phys., 14(16), 8579–8597, doi:10.5194/acp-14-8579-2014, 2014.

Van Der Does, M., Korte, L. F., Munday, C. I., Brummer, G. J. A. and Stuut, J. B. W.: Particle size traces modern Saharan dust transport and deposition across the equatorial North Atlantic, Atmos. Chem. Phys., 16(21), 13697–13710, doi:10.5194/acp-16-13697-2016, 2016.

Clift, R. and Gauvin, W. H.: Motion of entrained particles in gas streams, Can. J. Chem. Eng., 49(4), 439–448, doi:10.1002/cjce.5450490403, 1971.

Grell, G. A., Peckham, S. E., Schmitz, R., McKeen, S. A., Frost, G., Skamarock, W. C. and Eder, B.: Fully coupled "online" chemistry within the WRF model, Atmos. Environ., 39(37), 6957–6975, doi:10.1016/j.atmosenv.2005.04.027, 2005.

Hilsenrath, J. and of Standards, U. S. N. B.: Tables of Thermal Properties of Gases: Comprising Tables of Thermodynamic and Transport Properties of Air, Argon, Carbon Dioxide, Carbon Monoxide, Hydrogen, Nitrogen, Oxygen, and Steam, U.S. Department of Commerce, National Bureau of Standards. [online] Available from: https://books.google.gr/books?id=LK8vaddchE4C, 1955.

Huang, Y., Kok, J. F., Kandler, K., Lindqvist, H., Nousiainen, T., Sakai, T., Adebiyi, A. and Jokinen, O.: Climate Models and Remote Sensing Retrievals Neglect Substantial Desert Dust Asphericity, Geophys. Res. Lett., 47(6), 1–11, doi:10.1029/2019GL086592, 2020.

Kandler, K., et al.: Size distribution, mass concentration, chemical and mineralogical composition and derived optical parameters of the boundary layer aerosol at Tinfou, Morocco, during SAMUM 2006, Tellus B, 61, 32–50, https://doi.org/10.1111/j.1600-0889.2008.00385.x, 2009.

Mallios, S. A., Drakaki, E. and Amiridis, V.: Effects of dust particle sphericity and orientation on their gravitational settling in the earth's atmosphere, J. Aerosol Sci., 150(April), 105634, doi:10.1016/j.jaerosci.2020.105634, 2020.

Meng, J., Huang, Y., Leung, D. M., Li, L., Adebiyi, A. A., Ryder, C. L., Mahowald, N. M. and Kok, J. F.: Improved Parameterization for the Size Distribution of Emitted Dust Aerosols Reduces Model Underestimation of Super Coarse Dust, Geophys. Res. Lett., 49(8), e2021GL097287, doi:https://doi.org/10.1029/2021GL097287, 2022.

U.S. Standard Atmosphere, 1962, U.S. Government Printing Office, Washington, D.C., 1962,https://www.ngdc.noaa.gov/stp/space-weather/online-publications/miscellaneous/us-standard-atmosphere-1976/us-standard-atmosphere_st76-1562_noaa.pdf

Roberts, A. J., Marsham, J. H., Knippertz, P., Parker, D. J., Bart, M., Garcia-Carreras, L., Hobby, M., McQuaid, J. B., Rosenberg, P. D. and Walker, D.: New Saharan wind observations reveal substantial biases in analysed dust-generating winds, Atmos. Sci. Lett., 18(9), 366–372, doi:10.1002/asl.765, 2017.

Ryder, C. L., Highwood, E. J., Lai, T. M., Sodemann, H. and Marsham, J. H.: Impact of atmospheric transport on the evolution of microphysical and optical properties of Saharan dust, Geophys. Res. Lett., 40(10), 2433–2438, doi:10.1002/grl.50482, 2013

Ryder, C. L., Marenco, F., Brooke, J. K., Estelles, V., Cotton, R., Formenti, P., McQuaid, J. B., Price, H. C., Liu, D., Ausset, P., Rosenberg, P. D., Taylor, J. W., Choularton, T., Bower, K., Coe, H., Gallagher, M., Crosier, J., Lloyd, G., Highwood, E. J. and Murray, B. J.: Coarse-mode mineral dust size distributions, composition and optical properties from AER-D aircraft measurements over the tropical eastern Atlantic, Atmos. Chem. Phys., 18(23), 17225–17257, doi:10.5194/acp-18-17225-2018, 2018.

Ryder, C. L., Highwood, E. J., Walser, A., Seibert, P., Philipp, A. and Weinzierl, B.: Coarse and giant particles are ubiquitous in Saharan dust export regions and are radiatively significant over the Sahara, Atmos. Chem. Phys., 19(24), 15353–15376, doi:10.5194/acp-19-15353-2019, 2019.

Solomos, S., Kalivitis, N., Mihalopoulos, N., Amiridis, V., Kouvarakis, G., Gkikas, A., Binietoglou, I., Tsekeri, A., Kazadzis, S., Kottas, M., Pradhan, Y., Proestakis, E., Nastos, P. T. and Marenco, F.: From tropospheric folding to Khamsin and Foehn winds: How atmospheric dynamics advanced a record-breaking dust episode in Crete, Atmosphere (Basel)., 9(7), doi:10.3390/atmos9070240, 2018.

Versteeg H. K. & Malalasekera W. (2007). An introduction to computational fluid dynamics : the finite volume method (2nd ed.). Pearson Education.